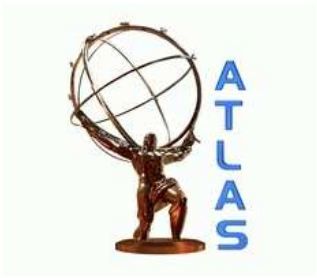

ATLAS NOTE

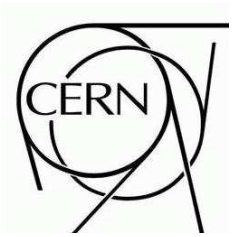

May 19, 2009

Discovery Potential for Supersymmetry with *b*-jet Final States with the ATLAS detector

The ATLAS Collaboration

ATL-PHYS-PUB-2009-075
25 May 2009

Abstract

This analysis describes the ATLAS discovery potential for supersymmetry in inclusive searches with *b*-jets in the final state, assuming a luminosity of 1 fb^{-1}and a center of mass energy of 14 TeV. The different sources of backgrounds and the expected uncertainties in their determination are considered. The discovery potential is addressed in a mSUGRA model at large $\tan\beta$ and it is found to be competitive with other inclusive searches, especially at high m_0 values.

1 Introduction

Supersymmetry (SUSY) [1] with R-parity conservation is one of the most theoretically motivated extensions of the Standard Model (SM) [2]. This theory predicts the existence of new particles such as squarks and gluinos, which are the superpartners of quarks and gluons. These particles could be produced in proton-proton collisions at the LHC and then would decay producing a striking signature of multiple high energetic jets, large missing transverse energy ($E_{\mathrm{T}}^{\mathrm{miss}}$) and possibly leptons. One of the goals of the LHC is to search for the existence of such supersymmetric particles. The first step in this quest is finding an excess in characteristic distributions with respect to the SM predictions. Due to the rich phenomenology that SUSY predicts, it is important to establish this excess in as many channels as possible.

In recent studies [3], the discovery potential for SUSY was carefully evaluated in a variety of possible channels. However, final states with *b*-jets and $E_{\mathrm{T}}^{\mathrm{miss}}$ were not fully addressed. These final states are particularly relevant in some regions of gravity mediated SUSY breaking models (mSUGRA) [4], where the SUSY parameter space can be determined by five parameters (m_0, $m_{1/2}$, A_0, $\tan\beta$ and sign(μ)). For large $\tan\beta$, the mixing of weak eigenstates is such that the mass of the *b*-quark superpartner is significantly lower than the ones from the first and second generations. This enhances its production and leads to decays with *b*-jets in the final state.

The purpose of this analysis is to assess the ATLAS discovery potential for this particular signature. First, the Monte Carlo (MC) samples used for the simulation of the signals and backgrounds are summarised. Two proposed event selections requiring two and three *b*-jets in the final state are described. Then, the method to determine the discovery potential is described and results are discussed.

2 Monte Carlo Samples

2.1 Signal

The signal under study was inclusive SUSY production, especially at large $\tan\beta$. For that purpose, a mSUGRA (m_0, $m_{1/2}$)-grid was considered with $\tan\beta = 50$, $A_0 = 0$ and $\mu > 0$. The grid range is 200 GeV $< m_0 <$ 2600 GeV, in steps of 200 GeV, and 100 GeV $< m_{1/2} <$ 1100 GeV, in steps of 100 GeV. At each point the signal events were generated using HERWIG 6.510 [5] interfaced to ISAJET 7.75 [6], to determine the particle spectrum. A fast simulation of the ATLAS detector, ATLFAST-I [7], was used. This simulation uses a simplified detector geometry and parametrisations of the detector response to increase the simulation speed. Some further corrections were derived from a comparison to a detailed GEANT-based detector simulation at a reference point on the grid. The leading-order (LO) cross-sections[1)] obtained from HERWIG for each grid point are shown in Fig. 1. The region marked with "NO EWSB" is theoretically excluded since no electroweak symmetry breaking is possible. In the region marked with "$\tilde{\tau}_1$ LSP" the $\tilde{\tau}_1$ would be the lightest supersymmetric particle (LSP). This region is disfavoured due to the constraints of having a charged Dark Matter candidate and, therefore, it is excluded from the region of interest. Lines with fixed gluino and squark masses are also indicated in the figure. Here, the squark mass was taken as the lightest one, considering the first and second squark generations only.

Two mSUGRA points with different $\tan\beta$ values were taken as reference. The one with a low $\tan\beta$ value is named SU3 ($m_0 = 100$ GeV, $m_{1/2} = 300$ GeV, $A_0 = -300$ GeV, $\tan\beta = 6$, $\mu > 0$) and the one with large $\tan\beta$ is called SU6 ($m_0 = 320$ GeV, $m_{1/2} = 375$ GeV, $A_0 = 0$, $\tan\beta = 50$, $\mu > 0$).

[1)] The use of LO cross-sections for signal is a conservative approach to determine the discovery potential.

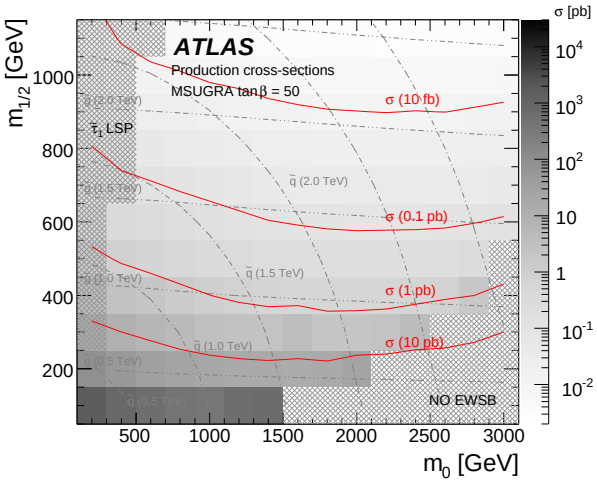

Fig. 1: Leading order cross-sections for points in the mSUGRA grid for $\tan\beta = 50$, $A_0 = 0$ and $\mu > 0$. The regions where no electroweak symmetry breaking is possible and where the $\tilde{\tau}_1$ is the LSP are also shown, together with lines with constant gluino and squark masses (using the lightest squark from the first or second generation).

For both points, events were simulated using detailed GEANT-4 and ATLFAST-I. Unlike the mSUGRA grid case, the corresponding inclusive cross-sections for these reference points were calculated at next-to-leading order (NLO) using Prospino2 [8] to be 27.7 pb (SU3) and 6.07 pb (SU6).

2.2 Background processes

For this analysis, the expected signature is characterised by a high jet multiplicity, missing transverse energy and b-jets. As in similar SUSY studies the dominant background is $t\bar{t}$-production. Other relevant backgrounds are multi-jet QCD processes, W+jet, Z+jet, associated W production with b-jets ($Wb\bar{b}$) and diboson production. All background processes were simulated using a full GEANT-4 detector simulation. A detailed description can be found in the SUSY chapter of Ref. [9]. The main characteristics are summarised in Table 1. Top pair production was generated using MC@NLO [10] and the process was separated at truth level according to whether at least one of the W decays leptonically or both fully hadronically. The sample was normalised to NLO including NLL resummation of soft effects [11]. The multi-jet QCD processes were generated with PYTHIA in different p_{T} ranges and normalised to LO. In addition, a filter at generator level was applied to achieve an increase of statistics in the interesting region of the analysis: $p_{\mathrm{T}}(\mathrm{jet}_1) > 80$ GeV, $p_{\mathrm{T}}(\mathrm{jet}_2) > 40$ GeV and $E_{\mathrm{T}}^{\mathrm{miss}} > 100$ GeV[2)]. The associated production of W or Z bosons and jets was generated using ALPGEN [12] and HERWIG. A filter at truth level was also applied requiring four jets with $p_{\mathrm{T}} > 40$ GeV, $p_{\mathrm{T}}(\mathrm{jet}_1) > 80$ GeV and $E_{\mathrm{T}}^{\mathrm{miss}} > 80$ GeV. The overall cross-sections were normalised to NNLO using FEWZ [13]. Diboson processes were generated with HERWIG and normalised to the corresponding NLO cross-sections calculated by MCFM [14]. Finally, in the present study the $Wb\bar{b}$ background was also considered, using the same generator and normalisation procedure as for W+jet production. This background, together with the associated Z production with b-jets ($Zb\bar{b}$) could have a significant contribution to the signature under study[3)]. $Zb\bar{b}$ was not available when performing this study and it has

[2)] A jet at generator level uses a cone 0.4 algorithm over all the stable particles, excluding neutrinos and muons.

[3)] Considering $Wb\bar{b}$ independently from W+jet can lead to some double counting of events. However, this is considered to be a conservative estimation, here.

not been considered. Its contribution is foreseen to be of the same order or lower than the $Wb\bar{b}$ contribution, given the different cross-sections and the probabilities of producing large missing transverse energy and multiple jets.

Background	Generator	σ_{eff} [pb]	L [pb^{-1}]
$t\bar{t}$ with leptons	MC@NLO	450	971
$t\bar{t}$ without leptons	MC@NLO	383	188
Multi-jets ($140 < p_{\mathrm{T}} < 280$ GeV)	PYTHIA	916	74.2
Multi-jets ($280 < p_{\mathrm{T}} < 560$ GeV)	PYTHIA	655	140
Multi-jets ($560 < p_{\mathrm{T}} < 1120$ GeV)	PYTHIA	67.4	477
Multi-jets ($1120 < p_{\mathrm{T}} < 2240$ GeV)	PYTHIA	5.3	660
Multi-jets ($p_{\mathrm{T}} > 2280$ GeV)	PYTHIA	0.022	$1.92 \cdot 10^5$
$W \to e\nu$+ 2 partons	ALPGEN+HERWIG	0.768	977
$W \to e\nu$+ 3 partons	ALPGEN+HERWIG	3.90	$4.04 \cdot 10^3$
$W \to e\nu$+ 4 partons	ALPGEN+HERWIG	2.32	$4.27 \cdot 10^3$
$W \to e\nu$+ 5 partons	ALPGEN+HERWIG	0.685	$4.31 \cdot 10^3$
$W \to \mu\nu$+ 3 partons	ALPGEN+HERWIG	0.799	$2.50 \cdot 10^3$
$W \to \mu\nu$+ 4 partons	ALPGEN+HERWIG	2.13	469
$W \to \mu\nu$+ 5 partons	ALPGEN+HERWIG	0.701	$5.71 \cdot 10^3$
$W \to \tau\nu$+2 partons	ALPGEN+HERWIG	0.615	$4.47 \cdot 10^3$
$W \to \tau\nu$+3 partons	ALPGEN+HERWIG	3.27	535
$W \to \tau\nu$+4 partons	ALPGEN+HERWIG	3.08	$4.55 \cdot 10^3$
$W \to \tau\nu$+5 partons	ALPGEN+HERWIG	0.935	$5.03 \cdot 10^3$
$Z \to ee$+1 parton	ALPGEN+HERWIG	0.401	$3.74 \cdot 10^3$
$Z \to ee$+2 partons	ALPGEN+HERWIG	4.15	$1.46 \cdot 10^3$
$Z \to ee$+3 partons	ALPGEN+HERWIG	2.76	$7.92 \cdot 10^3$
$Z \to ee$+4 partons	ALPGEN+HERWIG	0.694	$8.64 \cdot 10^3$
$Z \to ee$+5 partons	ALPGEN+HERWIG	0.176	$1.14 \cdot 10^4$
$Z \to \mu\mu$+3 partons	ALPGEN+HERWIG	0.240	$8.32 \cdot 10^3$
$Z \to \mu\mu$+4 partons	ALPGEN+HERWIG	0.527	$4.17 \cdot 10^3$
$Z \to \mu\mu$+5 partons	ALPGEN+HERWIG	0.170	$1.03 \cdot 10^4$
$Z \to \tau\tau$+2 partons	ALPGEN+HERWIG	0.215	$1.74 \cdot 10^4$
$Z \to \tau\tau$+3 partons	ALPGEN+HERWIG	0.411	$1.70 \cdot 10^4$
$Z \to \tau\tau$+4 partons	ALPGEN+HERWIG	0.207	$1.93 \cdot 10^4$
$Z \to \tau\tau$+5 partons	ALPGEN+HERWIG	0.062	$1.62 \cdot 10^4$
$Z \to \nu\nu$+3 partons	ALPGEN+HERWIG	1.07	$1.07 \cdot 10^4$
$Z \to \nu\nu$+4 partons	ALPGEN+HERWIG	3.06	$8.50 \cdot 10^3$
$Z \to \nu\nu$+5 partons	ALPGEN+HERWIG	0.951	$1.21 \cdot 10^4$
Diboson WW	HERWIG	39.0	$1.26 \cdot 10^3$
Diboson ZZ	HERWIG	2.81	$2.39 \cdot 10^4$
Diboson WZ	HERWIG	14.0	$3.49 \cdot 10^3$

Table 1: Main characteristics of the samples used in this analysis: the generators, the cross-sections after filter and matching efficiencies when applicable and the sample luminosities. The cross-sections were calculated as described in the main text.

3 Event selection

Jets were reconstructed using a seeded cone algorithm [15] with radius $\Delta R = \sqrt{\Delta\eta^2 + \Delta\phi^2} = 0.4$ over the calorimeter towers. Kinematic cuts requiring $p_{\mathrm{T}} > 20$ GeV and $|\eta| < 2.5$ are applied. To identify b-jets, the default ATLAS b-tagging algorithm (IP3DSV1, as described in Ref. [16]) was used. A b-tag weight greater than 6.75 was chosen. This value was extracted from $t\bar{t}$ studies and corresponds to a b-tagging efficiency of $\sim 60\%$ and to a rejection of ~ 100 (~ 10) against light-quark (c-quark) jets. Isolated electrons and muons were identified using the corresponding standard ATLAS algorithms with 'medium' requirements. Cuts on $p_{\mathrm{T}} > 20$ GeV and $|\eta| < 2.5$ were applied to both objects. In addition, events with electrons in the crack region between the central and endcap calorimeters ($1.37 < |\eta| < 1.52$) were removed. Finally, the missing transverse energy was corrected for the different calibrations of the calorimetric objects and for the muons.

In this study, two additional quantities used to discriminate signal against background were also considered:

- The transverse sphericity S_{T} was computed using the 2×2 sphericity tensor $S_{ij} = \sum_k p_{ki} p_j^k$ including all jets and isolated leptons:
$$S_{\mathrm{T}} = \frac{2\lambda_2}{\lambda_1 + \lambda_2}$$
where λ_1 and λ_2 are the eigenvalues of S_{ij}.
- The effective mass (M_{eff}) was defined as the scalar sum of the four highest p_{T} jets, leptons and the missing transverse energy:
$$M_{eff} = E_{\mathrm{T}}^{\mathrm{miss}} + \sum_{i=1}^{4} p_{\mathrm{T}}(\mathrm{jet}_i) + \sum p_{\mathrm{T}}(\mathrm{leptons})$$

After a detailed study on signal and background characteristics, two event selections characterised by the number of b-jets were adopted: a *2 b-jets* and a *3 b-jets* event selections.

2 b-jets selection The 2 b-jets event selection was inspired by the optimisation performed in previous studies [9][4]:

1. At least 4 jets with $p_{\mathrm{T}} > 50$ GeV
2. $p_{\mathrm{T}}(\mathrm{jet}_1) > 100$ GeV
3. $E_{\mathrm{T}}^{\mathrm{miss}} > 100$ GeV
4. $E_{\mathrm{T}}^{\mathrm{miss}} > 0.2\, M_{eff}$
5. $S_{\mathrm{T}} > 0.2$
6. At least 2 b-jets
7. $\Delta\varphi(\mathrm{jet}_{1,2,3}, E_{\mathrm{T}}^{\mathrm{miss}}) > 0.2$

The first three cuts are motivated by the fact that large jet multiplicities and large $E_{\mathrm{T}}^{\mathrm{miss}}$ are powerful discriminators against the background. In addition, these cuts ensure that the trigger inefficiency is minimised[5]. Cut 4 was introduced to reject backgrounds where the $E_{\mathrm{T}}^{\mathrm{miss}}$ is not significant in the final states, as in multi-jet processes. Cut 5 selects events with a tendency to have a more spherical topology in the transverse plane and cut 6 defines the 2 b-jets channel.

[4] Although the $E_{\mathrm{T}}^{\mathrm{miss}}$ threshold could underestimate the multijet QCD contribution due to the truth filter thresholds, this effect was found to be completely negligible after the other cuts are applied.

[5] In this study the small trigger inefficiency was neglected.

Finally, cut 7 removes events where the azimuthal distance between the $E_{\mathrm{T}}^{\mathrm{miss}}$ and one of the three highest jets in p_{T} is below 0.2. This cut was introduced to have a better control of the multi-jet background, where large $E_{\mathrm{T}}^{\mathrm{miss}}$ could rise from a mismeasured jet.

The number of accepted signal and background events assuming an integrated luminosity of 1 fb^{-1}are shown in Table 2 and 3 for the signal reference points SU3 and SU6 and for the various backgrounds. As can be seen, cuts 4 and 7 are powerful discriminators against the multi-jet background processes. The requirement of 2 b-jets in the final state removes large parts of W and Z backgrounds while keeping most of the signal, especially in the case of SU6 since b-jet final states are more probable at large $\tan\beta$ environments.

cut	$t\bar{t}$	QCD	W+jet	Z+jet	W$b\bar{b}$	Diboson
1-3	$(1.29 \pm 0.01)\cdot 10^4$	$(2.97 \pm 0.05)\cdot 10^4$	$(4.07 \pm 0.05)\cdot 10^3$	$(1.63 \pm 0.01)\cdot 10^3$	121 ± 12	23 ± 3
4	$(8.28 \pm 0.09)\cdot 10^3$	$(6.74 \pm 0.29)\cdot 10^3$	$(2.31 \pm 0.04)\cdot 10^3$	$(1.04 \pm 0.01)\cdot 10^3$	71 ± 9	14 ± 3
5	$(6.12 \pm 0.08)\cdot 10^3$	$(4.25 \pm 0.23)\cdot 10^3$	$(1.60 \pm 0.34)\cdot 10^3$	729 ± 9	53 ± 8	9 ± 2
6	$(2.17 \pm 0.05)\cdot 10^3$	748 ± 99	23 ± 4	9 ± 1	11 ± 4	2 ± 1
7	$(1.94 \pm 0.05)\cdot 10^3$	225 ± 54	22 ± 4	8 ± 1	10 ± 3	2 ± 1

Table 2: Number of expected background events, including the statistical uncertainties and assuming an integrated luminosity of 1 fb^{-1}.

cut	SU3	SU6	SM bkg.
1-3	$(9.60 \pm 0.02)\cdot 10^3$	$(2.55 \pm 0.02)\cdot 10^3$	$(4.84 \pm 0.06)\cdot 10^4$
4	$(7.46 \pm 0.02)\cdot 10^3$	$(2.02 \pm 0.02)\cdot 10^3$	$(1.84 \pm 0.03)\cdot 10^4$
5	$(5.57 \pm 0.02)\cdot 10^3$	$(1.45 \pm 0.02)\cdot 10^3$	$(1.27 \pm 0.02)\cdot 10^4$
6	$(1.10 \pm 0.01)\cdot 10^3$	499 ± 10	$(2.97 \pm 0.11)\cdot 10^3$
7	$(1.03 \pm 0.01)\cdot 10^3$	471 ± 10	$(2.21 \pm 0.07)\cdot 10^3$

Table 3: Number of expected events for signal and total SM background, including the statistical uncertainties and assuming an integrated luminosity of 1 fb^{-1}.

After all selection cuts, the $t\bar{t}$ process is the main background to this search, followed by multi-jet QCD processes (one order of magnitude below). Other backgrounds like W/Z+jet, W$b\bar{b}$ and diboson are less important. However, looking at Fig. 2, where the M_{eff} distribution is shown after all the cuts for the SU6 mSUGRA reference point and all the backgrounds, one can observe that $t\bar{t}$ and multi-jet QCD processes tend to contribute at lower M_{eff} regions, whereas W and Z contributions have a slightly different shape that extends towards higher M_{eff} values.

In Table 4 the percentages of events with at least one or at least two true b-jets after cut 6 are presented. The true b-jets are identified as such if a b-quark with $p_{\mathrm{T}} > 5$ GeV is found, after final state radiation, within $\Delta R = 0.3$ of the candidate jet (defined with $p_{\mathrm{T}} > 20$ GeV and $|\eta| < 2.5$). The W+jet and Z+jet background contributions are the ones having the smallest number of true b-jets, although non negligible due to gluon splitting processes. This gluon splitting may also contribute to the high percentage of QCD events with true b-jets. Finally, all the remaining diboson and W$b\bar{b}$ contributions have two b-jets after the cuts but due to low statistics a 95% CL lower limit was set. As expected, SU6 has a larger number of b-jets in its final states than SU3 due to the different SUSY mass spectrum. The numbers obtained show that the channel is dominated by real b-jets.

3 b-jets selection Given the high b-jet multiplicity in the final states in some regions of the mSUGRA parameter space, a 3 b-jets selection, with the rest of the cuts as in the 2 b-jets case,

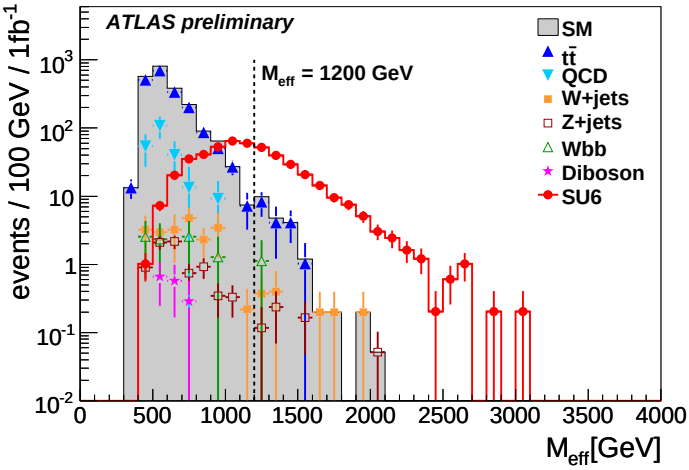

Fig. 2: M_{eff} distribution after the 2 b-jets event selection. The different background contributions are shown, together with the total SM background contribution and SU6 as a reference mSUGRA point. The $M_{eff} = 1200$ GeV value is also marked for its special role in the discovery potential calculation. All uncertainties are only statistical and an integrated luminosity of 1 fb^{-1}is assumed.

	1 b-jet [%]	2 b-jets [%]
$t\bar{t}$	≈ 100	95.2
QCD	96.4	88.2
W+jet	60.5	46.5
Z+jet	69.7	47.2
W$b\bar{b}$	> 71.7	> 71.7
Diboson	> 65.2	> 65.2
SU3	96.5	89.7
SU6	99.1	93.6

Table 4: Percentage of events with at least one or at least two true b-jets after cut 6 (requiring two reconstructed b-jets). True b-jet definition is described in the text. For the W$b\bar{b}$ and diboson background, a 95% CL lower limit is shown instead, due to low statistics.

was also proposed. This requirement reduces substantially the backgrounds and keeps the $t\bar{t}$ background as nearly the only one relevant for the search. A comparison between the expected number of background events after the two and the three b-jets selection is shown in Table 5.

Backgrounds	2 b-jets	Rel. Contrib.	3 b-jets	Rel. Contrib.
$t\bar{t}$	$(1.94 \pm 0.05)\cdot 10^3$	88.0%	189 ± 14	91.7%
QCD	225 ± 55	10.2%	14 ± 14	6.5%
W+jet	21.6 ± 4.5	1.0%	1.0 ± 0.6	0.5%
Z+jet	8.1 ± 0.9	0.4%	1.1 ± 0.3	0.5%
$Wb\bar{b}$	9.9 ± 3.5	0.4%	1.3 ± 1.3	0.6%
Diboson	1.5 ± 0.7	0.1%	0.3 ± 0.3	0.1%
SM	$(2.21 \pm 0.07)\cdot 10^3$	100%	207 ± 20	100%

Table 5: Number of expected background events for the 2 and 3 b-jets selections and the corresponding percentage to the overall SM expected events, assuming a luminosity of 1 fb^{-1}.

Table 6 shows the effect of applying the 3 b-jets requirement to the two signal reference points (SU3 and SU6), to another signal point, P_h, defined at large m_0 ($m_0 = 2000$ GeV, $m_{1/2} = 200$ GeV) from the generated grid and to the total SM background. In addition, the reduction of expected number of events with respect to the 2 b-jets channel is also shown. In all the cases, the background reduction when requiring 3 b-jets is higher than for signal. As expected, the new constraint is reducing more events from low $\tan\beta$ points. In addition, the events at higher m_0 have also a higher acceptance. One of the reasons is that once four jets in the event are required, the gluino-gluino production is dominant at this region and the main decay of the gluino is a three-body decay via a top, a bottom and a chargino, which enhances the b-jet multiplicity.

	2 b-jets	3 b-jets	3 b-jets/ 2 b-jets
SU3 ($\tan\beta = 6$, $m_0 = 100$ GeV, $m_{1/2} = 300$ GeV))	$(1.03 \pm 0.01)\cdot 10^3$	178 ± 3	0.17
SU6 ($\tan\beta = 50$, $m_0 = 320$ GeV, $m_{1/2} = 375$ GeV))	471 ± 10	124 ± 5	0.26
P_h ($\tan\beta = 50$, $m_0 = 2000$ GeV, $m_{1/2} = 200$ GeV))	$(1.01 \pm 0.01)\cdot 10^3$	418 ± 33	0.41
SM bkg.	$(2.21 \pm 0.07)\cdot 10^3$	207 ± 20	0.09

Table 6: Number of expected events after the 2 and 3 b-jets event selection for the total SM background and three signal points with different $\tan\beta$ and m_0 values. The ratios between the 3 and 2 b-jets are also shown. Uncertainties are only statistical and an integrated luminosity of 1 fb^{-1}is assumed.

4 Systematic uncertainties

The MC estimation of the M_{eff} shapes and the normalisations of the different backgrounds have large uncertainties associated. Thus, a number of techniques were developed [9] to estimate the different background contributions from data. The uncertainties of the method were studied and estimated to be about 50% for QCD multi-jet processes and 20% for the $t\bar{t}$ and electroweak backgrounds, assuming 1 fb^{-1}of collected data. In case of the $t\bar{t}$ estimation, b-tagging efficiency uncertainties were considered. Since the present study relies heavily on b-tagging, additional b-tagging systematic uncertainties were taken into account. This implies that for the $t\bar{t}$ case, these uncertainties are over-estimated. The systematic uncertainty on b-tagging efficiency was calculated by removing 5% of true b-jets. The systematic uncertainty on rejection was considered by removing or adding 50% of fake b-jets and taking the maximal difference with respect to the nominal. Table 7 shows the final expected number of events for all backgrounds with the corresponding statistical and systematic uncertainties (showing separately the particular b-tagging uncertainties estimated in this study). It can be seen that in the 2 b-jets case, the systematic uncertainties derived from the data-driven estimation are significantly exceeding the b-jet systematic uncertainties in the case of the $t\bar{t}$ and QCD backgrounds. This is not the case in the 3 b-jets selection, where the fake b-tags constitute the dominant uncertainty. In order to assess the overall systematic uncertainties in the discovery potential calculation, both systematics were added in quadrature. In cases where the number of simulated events is too low to determine the b-tagging uncertainty (cases of W and Z, for 3 b-jets, and Wbb and diboson for both 2 and 3 b-jets), an overall systematic uncertainty of 100% was considered.

5 Method to determine the discovery potential

The procedure to determine the discovery potential is described in detail in Ref. [9] and will only be summarised here. For every point in the mSUGRA grid the significance Z_n (in terms of

	2 b-jets			3 b-jets		
	events (stat)	(sys)	(b-sys)	events (stat)	(sys)	(b-sys)
$t\bar{t}$	$(1.94 \pm 0.05$	± 0.39	$\pm 0.21) \cdot 10^3$	189 ± 14	± 38	± 91
QCD	225 ± 55	± 112	± 26	14 ± 14	± 7	± 14
W+jet	21.6 ± 4.5	± 4.3	± 7.8	1.0 ± 0.6	± 0.2	± 0.6
Z+jet	8.1 ± 0.9	± 1.6	± 2.9	1.1 ± 0.3	± 0.2	± 0.5
W$b\bar{b}$	9.9 ± 3.5	± 2.0	± 1.1	1.3 ± 1.3	± 0.3	± 0.6
Diboson	1.5 ± 0.7	± 0.3	± 0.2	0.3 ± 0.3	± 0.1	± 0.1
SM bkg.	$(2.21 \pm 0.07$	± 0.40	$\pm 0.24) \cdot 10^3$	206 ± 20	± 38	± 92

Table 7: Number of expected events after cut 7, with the corresponding statistical and systematic uncertainties considered in this study as described in the text, assuming 1 fb^{-1}.

standard deviations) was calculated from the number of background events, N_b, uncertainties, δN_b, and the expected number of data events, N_{data} (sum of background plus signal events). The probability p that N_b fluctuates to at least N_{data} is given by:

$$p = A \int_0^\infty G(b; N_b, \delta N_b) \sum_{i=N_{data}}^{\infty} \frac{e^{-b} b^i}{i!} \quad db$$

where $G(b; N_b, \delta N_b)$ is the Gaussian probability density function and A a normalisation factor. The probability was transformed to the number of standard deviations Z_n via:

$$Z_n(p) = \mathrm{erf}^{-1}(1-2p) \cdot \sqrt{2}$$

N_b, δN_b and N_{data} were extracted from the corresponding M_{eff} distributions. Starting at a selected lower bin b_{min}, all events in the higher bins were counted. Thus, the N_b value was taken from the M_{eff} distribution of the total Standard Model background and N_{data} was calculated by adding to N_b expected signal contribution in the corresponding bins. The total statistical uncertainty was obtained by adding the statistical uncertainties of the corresponding bins quadratically for the total background. A systematic uncertainty was derived by adding the systematic uncertainties per bin linearly for every background separately, and then adding these results in quadrature to obtain the systematic uncertainty of the total background. In the end the statistical and systematic uncertainties were added in quadrature.

In contrast to the studies presented in Ref. [9], the lower bin b_{min} was fixed to a maximum value of 1200 GeV in order to add robustness to the analysis and to make it less sensitive to statistical fluctuations of signal and background events with high M_{eff} values. It should be noted that this provides a more conservative estimation of the discovery significance.

6 Discussion of results

The discovery potential curves for the two and three b-jet analyses are shown in Fig. 3. As a reference, the discovery potential for the multi-jet plus 0 lepton mode [9] is also shown. Although applying a more conservative method to estimate the contours, the discovery reach of the b-jet channels is comparable to that of the multi-jet plus 0 lepton mode, and is even higher at large m_0, where the 3 b-jets analysis seems more powerful than the two b-jets analysis. The reason is that, at large m_0, gluinos are lighter than any of the squarks so their production is enhanced. As discussed, gluinos decay to top and bottom quarks, together with the second neutralino. This gives a final state with large jet multiplicity and rich heavy flavour content, increasing the acceptance.

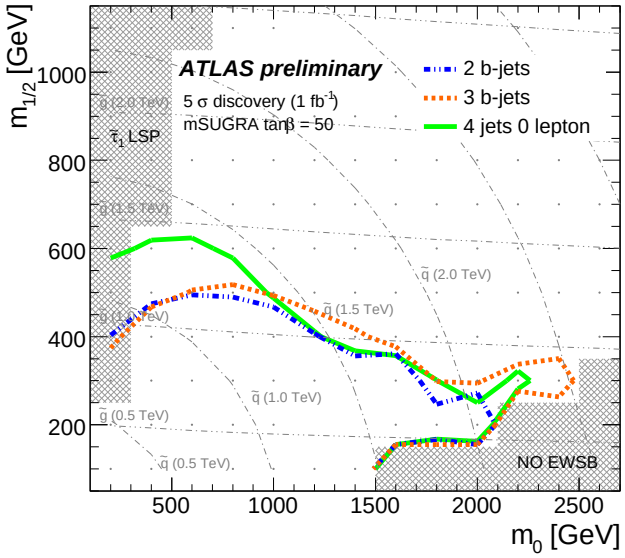

Fig. 3: The 5σ discovery potential contours in the mSUGRA $(m_0, m_{1/2})$-plane for $\tan\beta = 50$, $A_0 = 0$ and $\mu > 0$ for the 2 b-jets (semi-dashed, blue) and 3 b-jets (dashed, orange) analyses, assuming a luminosity of 1 fb^{-1}. As a reference, the multi-jet plus 0 lepton mode discovery potential result is also shown (solid, green) [9]. Lines with constant gluino and squark masses (using the lightest squark from the first or second generation) are also shown together with the theoretically excluded regions. The points chosen for simulation are indicated as dots.

Inclusive vs exclusive channels

Since the two proposed selections are inclusive in requesting different number of b-jets in the final state, there could be strong overlap between the results. The impact of this overlap is addressed in Fig. 4, where an exclusive 2 b-jets selection curve is also shown. In order to compute this curve, the same systematic uncertainties to that of the 2 b-jets inclusive mode were assumed.

As can be seen from the figure, the standard inclusive 2 b-jets contour is almost completely dominated by the presence of 3 b-jets, especially at large m_0 values. However, at lower m_0 values, the 2 b-jets exclusive curve has a comparable reach. Thus, in order to fully exploit this channel, two independent analyses could be defined and their sensitivities combined.

Discovery reach at a lower luminosity

The discovery potentials of the 2 and 3 b-jets analyses at a lower luminosity of 100 pb^{-1} are addressed in Fig. 5. Since lower luminosities increase the systematic uncertainty for the background, given the data-driven nature of their estimation and non-optimal b-tagging performance, the overall systematic uncertainty was doubled for each of the backgrounds with respect to the estimations discussed in Section 4.

The figure shows that even with 100 pb^{-1}, the discovery potential can reach m_0 values around 1500 GeV and $m_{1/2}$ values above 200 GeV. This indicates that it is an interesting channel to be considered already at the beginning of data-taking.

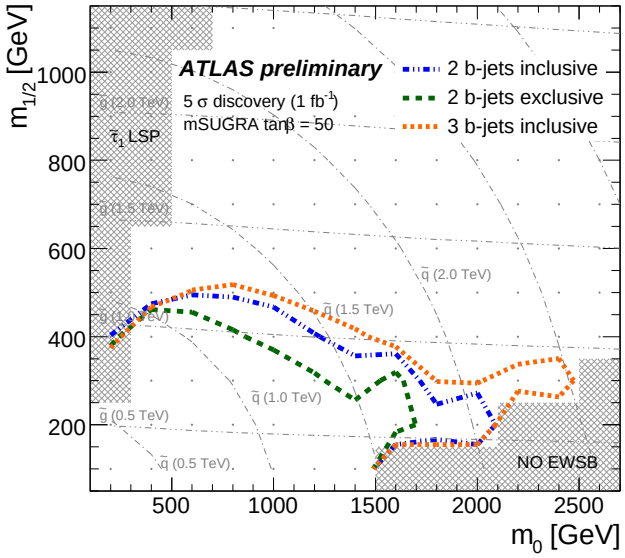

Fig. 4: The 5σ discovery potential contours in the mSUGRA $(m_0, m_{1/2})$-plane for $\tan\beta = 50$, $A_0 = 0$ and $\mu > 0$ with the inclusive 2 b-jets channel (requiring at least 2 b-jets) (semi-dashed, blue), the 2 b-jets channel defined exclusively (requiring no more than 2 b-jets) (dashed, dark green) and the inclusive 3 b-jets channel (requiring at least 3 b-jets) (dashed, orange) assuming a luminosity of 1 fb^{-1}.

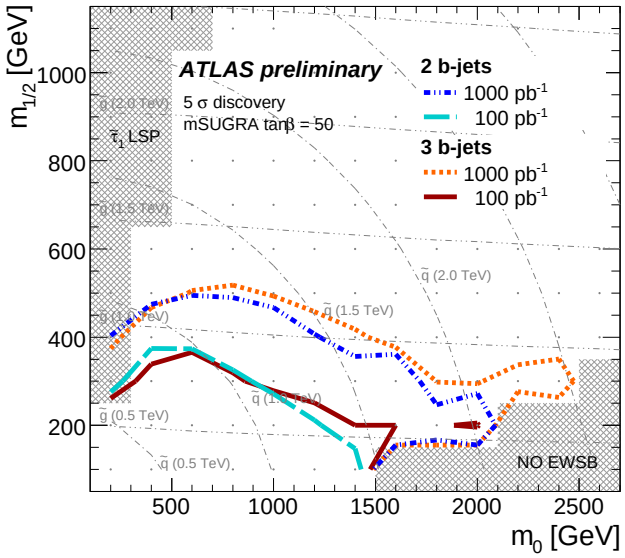

Fig. 5: The 5σ discovery potential contours in the the mSUGRA $(m_0, m_{1/2})$-plane for $\tan\beta = 50$, $A_0 = 0$ and $\mu > 0$ with the 2 b-jets and 3 b-jets analyses assuming 1000 pb^{-1} and 100 pb^{-1}.

7 Summary and conclusions

This study explored the ATLAS discovery potential for SUSY using inclusive b-jet modes. Requiring two and three b-jets in the final state reduces some backgrounds, like W and Z, and improves the signal over background ratio, especially for large $\tan\beta$-scenarios, where b-jets appear in the decays of coloured sparticles. The discovery potential for both the two and three b-jets channels is affected by systematic uncertainties on the background normalisation and

estimates. They have been constrained by applying data-driven methods together with a conservative estimation of the b-tagging systematics.

The discovery potential for these SUSY scenarios is comparable to the multi-jet plus 0 lepton mode, especially at large m_0, where the gluino undergoes a three body decay with b and t final states. Such richness of b-jets in the final state opens the possibility for a 3 b-jet analysis, where the background is much more reduced and still completely dominated by top production.

References

[1] S.P. Martin, *A supersymmetry primer*, hep-ph/9709356 (1997).

[2] S.L. Glashow, Nucl. Phys. **22** (1961) 579, S. Weinberg, Phys. Rev. Lett. **19** (1967) 1264, A. Salam, in Elementary Particle Theory, ed. N. Svartholm, Stockholm, "Almquist and Wiksell" (1968), 367.

[3] The ATLAS Collaboration, CERN-OPEN-2008-020 (2008).

[4] H.P. Nilles, Phys. Rep. **110** (1984) 1.

[5] G. Corcella and others, *HERWIG 6.5 release note*, hep-ph/0210213, 2002.

[6] F. Paige, S. Protopopescu, H. Baer and X. Tata, *ISAJET 7.69: A Monte Carlo event generator for p p, anti-p p, and e+ e- reactions*, hep-ph/0312045, 2003.

[7] Richter-Was, Elzbieta and Froidevaux, Daniel and Poggioli, Luc, *ATLFAST 2.0 a fast simulation package for ATLAS* Atlas Note ATL-PHYS-98-131.

[8] W. Beenakker, R. Hopker, M. Spira and P.M. Zerwas, Nucl. Phys. **B492** (1997) 51–103.

[9] The ATLAS Collaboration, CERN-OPEN-2008-020 (2008), p.1513.

[10] S. Frixione and B.R. Webber, JHEP **06** (2002) 029.

[11] R. Bonciani, S. Catani, M.L. Mangano and P. Nason, Nucl. Phys. **B529** (1998) 424–450.

[12] M. Mangano *et al.*, JHEP **07** (2003) 001.

[13] K. Melnikov and F. Petriello, Phys. Rev. **D74** (2006) 114017.

[14] J. Campbell, J. Ellis, User guide available at http://mcfm.fnal.gov/ (2007).

[15] The ATLAS Collaboration, CERN-OPEN-2008-020 (2008), p.261.

[16] The ATLAS Collaboration, CERN-OPEN-2008-020 (2008), p.397.